



OPEN

Characterization, in-silico, and in-vitro study of a new steroid derivative from *Ophiocoma dentata* as a potential treatment for COVID-19

Mohamed S. M. Abd El Hafez^{1,2✉}, Miral G. AbdEl-Wahab², Mohamed G. Seadawy³, Mostafa F. El-Hosseney³, Osama Beskales⁴, Ali Saber Ali Abdel-Hamid², Maha A. El Demellawy^{2,5} & Doaa A. Ghareeb^{2,6,7}

The medicinal potential of marine invertebrates' bioactive components that may act as anti-COVID-19 demonstrated promising results. *Ophiocoma dentata*, which is common in the Red Sea, is one such source. Therefore, this study aimed to isolate a new compound from the brittle star, *Ophiocoma dentata*, and evaluate its efficacy as anti-COVID-19 in-silico and in-vitro. Standard procedures were followed in order to assess the isolated compound's preliminary toxicity and anti-inflammatory properties. Computer virtual screening technology through molecular docking and ADMET studies was conducted as well as a new steroid derivative was isolated for the first time, named 5 α -cholesta-4(27), 24-dien-3 β , 23 β -diol. Investigation of the Anti-Covid-19 activity of the isolated compound using a Plaque reduction assay revealed 95% inhibition at a concentration of 5 ng/ μ l (12.48 μ M). Moreover, this compound showed an IC₅₀ of 11,350 \pm 1500 ng/ml against the normal fibroblast cells, indicating its safety. Interestingly, this compound exhibited anti-inflammatory activity with an IC₅₀ of 51.92 \pm 0.03 μ g/ml compared to a reference drug's IC₅₀ of 53.64 \pm 0.01 μ g/ml, indicating that this compound is a potent anti-inflammatory. In silico data have proved that the isolated compound is a promising viral inhibitor against SARS-CoV2 and is thus recommended as a future nature preventive and curative antiviral drug.

More than 5 million people have died due to the COVID-19 outbreak worldwide, which has inflicted political and socioeconomic disruptions in our daily lives¹. Researchers have started repurposing already FDA-approved medications for COVID-19 treatment as a quick method to reduce the time required for safety and approval studies². Currently, scientific efforts focus on developing a suitable medication from the old traditional pharmaceuticals used for earlier coronavirus strains³. Many natural product derivative treatments have been reported to prevent the entry and replication of various coronaviruses, such as SARS and MERS. Natural compounds and their molecular frameworks have long been considered valuable starting points or sources for drug discovery⁴.

Blunt et al.⁵ revealed that marine natural products are beneficial substances for drug discovery due to their wide variety of bioactivities, including anti-infective, anti-proliferative, antibiotic, and anti-tumor properties. Marine invertebrates generally are motionless and stuck to the ocean bottom, they use potent secondary metabolites to prevent the growth of invading neighbors and attract food. Such survival conditions stimulated the

¹National Institute of Oceanography and Fisheries (NIOF), Cairo, Egypt. ²Center of Excellence for Drug Preclinical Studies (CE-DPS), Pharmaceutical and Fermentation Industries Development Centre (PFIDC), City of Scientific Research and Technological Applications (SRTA-City), New Borg El Arab, Egypt. ³Biological Prevention Department, Egyptian Army, Cairo, Egypt. ⁴Medical Services Department, The Egyptian Army, Cairo, Egypt. ⁵Medical Biotechnology Department, Genetic Engineering & Biotechnology Research Institute, City of Scientific Research and Technological Applications (SRTA-City), New Borg El Arab, Egypt. ⁶Bio-screening and Preclinical Trial Lab, Biochemistry Department, Faculty of Science, Alexandria University, Alexandria, Egypt. ⁷Biochemistry Department, Faculty of Science, Alexandria University, Alexandria, Egypt. ✉email: mohamedsaid80@yahoo.com

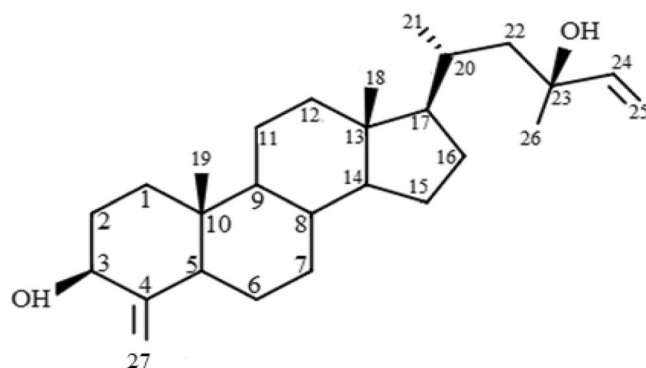


Figure 1. 5 α -cholesta-4(27), 24-dien-3 β , 23 β -diol isolated from the brittle star (*O. dentata*).

production of a highly abundant variety of biologically active substances⁵. Echinoderms demonstrate as an untapped source in an attempt to identify novel and beneficial products⁶. According to Fayed et al.⁷, marine natural products have demonstrated antiviral activity against coronaviruses, and various aquatic species have previously been discovered to produce a variety of antiviral lead compounds. Brittle stars (Ophiuroidea) are the largest echinoderm group in terms of species, as well as the most frequent⁸. There have been a few studies on the biological activity of brittle star species have been published. However, the antiviral activity of the brittle star revealed that the most abundant bioactive metabolites derived from brittle star are steroidal glycosides, carotenoid sulfates, and naphthoquinone. All of which are essential for life maintenance on earth and have the potential to be used in biomedicine⁸.

Molecular modeling and virtual screening are examples of computational-based techniques that contribute to understanding the molecular components of protein–ligand interactions throughout the rational drug discovery process^{9,10}. Two intriguing therapeutic targets for SARS-CoV-2 related disorders are the main protease (Mpro) and the RNA-dependent RNA polymerase (RdRP), which are responsible for the viral polyprotein proteolytic process along with viral genome replication and transcription^{11,12}. These two target sites have been intensively docked to develop or distinguish structure-based effective medicines for COVID-19 based on their critical role in the life cycle of SARS-CoV-2¹³. Natural bioactive compounds are currently being screened for their affinity for COVID-19 molecular targets using molecular docking, with the advantage that natural products are free of harmful or adverse effects^{14,15}. This study aims to isolate a new compound from the brittle stars, *Ophiocoma dentata* that can resist COVID-19. In addition, structure elucidation, anti-inflammatory activity, molecular docking and in silico ADMET studies were performed.

Results

Structure determination of the isolated compound. The new compound was obtained as yellow crystals, and HREIMS provided its molecular formula, C₂₇H₄₄O₂ (m/z 400.6470), indicating the presence of six degrees of unsaturation. In addition to the double bond (1742 cm⁻¹), the FTIR spectrum revealed the presence of hydroxyl (3424 cm⁻¹). ¹H NMR spectrum of the isolated compound showed the presence of one proton multiplet at δ 4.14, the position and multiplicity of which was indicative of H-3 of the steroidal nucleus. Presence of four methyl [δ 0.86 (3H, s, H-18), δ 1.19 (3H, s, H-19), δ 1.06 (3H, d, J = 10 Hz, H-21), δ 5.93 (3H, m, H-24)] and four-terminal olefinic protons [δ 5.09 and δ 4.93 (H-25 and H-27)].

The ¹³C NMR spectrum of the isolated compound revealed the resonance of 27 carbons identified as four methyls, ten methylene (including two terminal double bonds), one oxygenated methine, and five quaternary carbons. The isolated compound's complete ¹H and ¹³C NMR chemical shifts were assigned using a combination of COSY-45°, HSQC, and HMBC spectra. These spectroscopic studies suggested that the isolated compound had a steroidal type skeleton. Consequently, were proposed the structure for this new compound named 5 α -cholesta-4(27), 24-dien-3 β , 23 β -diol. ¹H NMR, ¹³C NMR, HSQC, HMBC, COSY, NOESY, and FTIR data are depicted in (Fig. 1 and supplementary Figs. S2–S8; Table S1).

Molecular docking, ADMET analysis, and in silico toxicity studies of the isolated compound. In this work, the binding potential of the isolated compound against three proteins of SARS-CoV-2 has been investigated. The selected proteins are: (i) COVID-19 main protease (M^{Pro}) (PDB ID: 6lu7, resolution: 2.16 Å), (ii) nonstructural protein (nsp)10 (PDB ID: 6W4H, resolution: 1.80 Å), and (iii) RNA-dependent RNA polymerase (PDB ID: 7BV2, resolution: 2.50 Å).

Re-docking processes of the co-crystallized ligands (PRD_002214, SAM, and F86) were preceded against the active pockets of COVID-19 main protease, NSP10, and RNA-dependent RNA polymerase, respectively, to validate the docking procedure. The calculated RMSD values between the re-docked poses and the co-crystallized ones were 3.10, 1.07, and 1.34, indicating the efficiency and validity of the docking processes (Fig. 2).

Determination of anti-SARS-CoV2, MTT cytotoxicity, and anti-inflammatory activity. The percent inhibition of various concentrations of the isolated compound against SARS-CoV2 is shown in (Table 1).

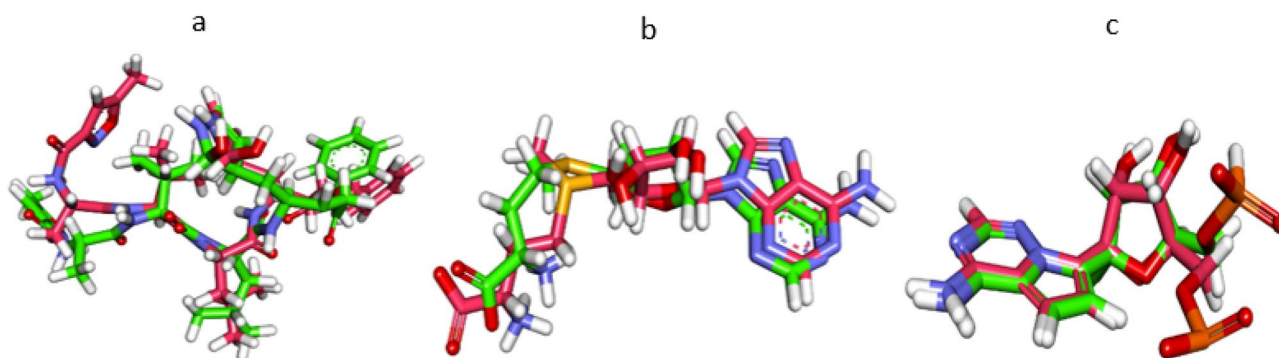


Figure 2. Superimposition of the co-crystallized pose and the docking pose of the same ligands. (a) PRD_002214 of COVID-19 main protease, (b) SAM of NSP10, (c) F86 of RNA-dependent RNA polymerase.

| Conc (ng/ μ l) | Initial viral count (PFU/ml) | Viral count (PFU/ml) | Inhibition % |
|--------------------|------------------------------|-------------------------------|--------------|
| 5 | 11 \times 10 ⁵ | 0.55 \times 10 ⁵ | 95 |
| 2.5 | | 0.88 \times 10 ⁵ | 92 |
| 1.25 | | 1.32 \times 10 ⁵ | 88 |
| 0.625 | | 1.65 \times 10 ⁵ | 85 |

Table 1. Anti-SARS-CoV2 activity of the isolated compound (Plaque Reduction Assay).

Interestingly, the isolated compound showed 95% viral inhibitory effects on SARS-CoV2 at a concentration of 5 ng/ μ l (12.48 μ M).

In this study, human gingival fibroblast cell lines (Fig. 3) were exposed to different concentrations of the isolated compound. The cellular responses were determined using in vitro toxicity MTT assay. The changes in the morphology of cells exposed to different concentrations of the isolated compound were monitored using inverted microscopy. The results demonstrated that the cells exposed to 12.5 μ g/ml of the isolated compound gradually lost their characteristic phenotype, started to shrink, and obtained irregular shapes. Percentage inhibition of the normal fibroblast cell growth at different concentrations of the isolated compound is shown in (supplementary Fig. S9), with an IC₅₀ value of 11.35 \pm 1.5 μ g/ml (0.02 mM).

The anti-inflammatory activity of the isolated compound of different concentrations (10, 40, 100, 400, and 600 μ g/ml) is shown in (Table 2).

Discussion

Chemical studies on *Ophiocoma dentata* have resulted in discovering a new steroid, 5 α -cholesta-4(27), 24-dien-3 β , 23 β -diol. The structure of the isolated compound was determined with the help of spectroscopic studies. The isolated compound's NMR spectra matched those of 5 α -cholesta-9(11),24- dien-3 β ,6 α ,20 β -triol-23-one 3-sulphate, reported by Yang et al.¹⁶, except for an absence of hydroxyl group at C-6, C-20 position and the double bond between C-9 and C-11 as well as additional double bond at C-4 and this was confirmed by the HMBC experiment. Inspection of its NMR data indicated a considerable similarity to those of ophidianoside F¹⁷ except for an absent hydroxyl group at C-6, C-20 and the double bond between C-9 and C-11, and the presence of a double bond between C-24 and C-25 position.

Docking studies were carried out using MOE14.0 software, yielding free energy (Δ G) values that indicate the examined molecule's binding interaction with the selected protein.

The isolated compound demonstrated good binding affinities with COVID-19 main protease (Δ G = - 24.68 kcal/mol), nsp10 (Δ G = - 23.47 kcal/mol), and RNA-dependent RNA polymerase (Δ G = - 29.86 kcal/mol), compared to the co-crystallized ligands PRD_002214 (Δ G = - 27.72 kcal/mol), SAM (Δ G = - 17.86 kcal/mol), and F86 (Δ G = - 23.56 kcal/mol), respectively (Table 3).

The docking mode of the co-crystallized ligand (PRD_002214) and COVID-19 main protease formed four hydrogen bonds and three hydrophobic interactions. The first pocket of M^{Pro} was occupied by 2-oxopyrrolidin-3-yl moiety, forming two hydrogen bonds with Thr190 and Gln189. Additionally, the isopropyl moiety occupied the second pocket of M^{Pro} forming three hydrophobic interactions with His41 and Met165. Furthermore, the third pocket was occupied by the benzyl acetate moiety, whereas the 5-methylisoxazole-3-carboxamide moiety was buried in the fourth pocket, forming a hydrogen bond with Thr26. Finally, one hydrogen bond was formed between an amide group and Met165 (supplementary Fig. S10).

Moreover, the co-crystallized ligand (SAM) formed three hydrogen bonds and seven hydrophobic interactions against the COVID-19 nsp10 protein. In detail, the tetrahydrofuran-3,4-diol moiety formed three hydrogen bonds with Asn6899, Tyr6930, and Asp6928. Besides, the 9H-purin-6-amine moiety formed three hydrophobic interactions with Phe6947 and Leu6898. Also, the (S)-(3-amino-3-carboxypropyl) dimethylsulfonium moiety

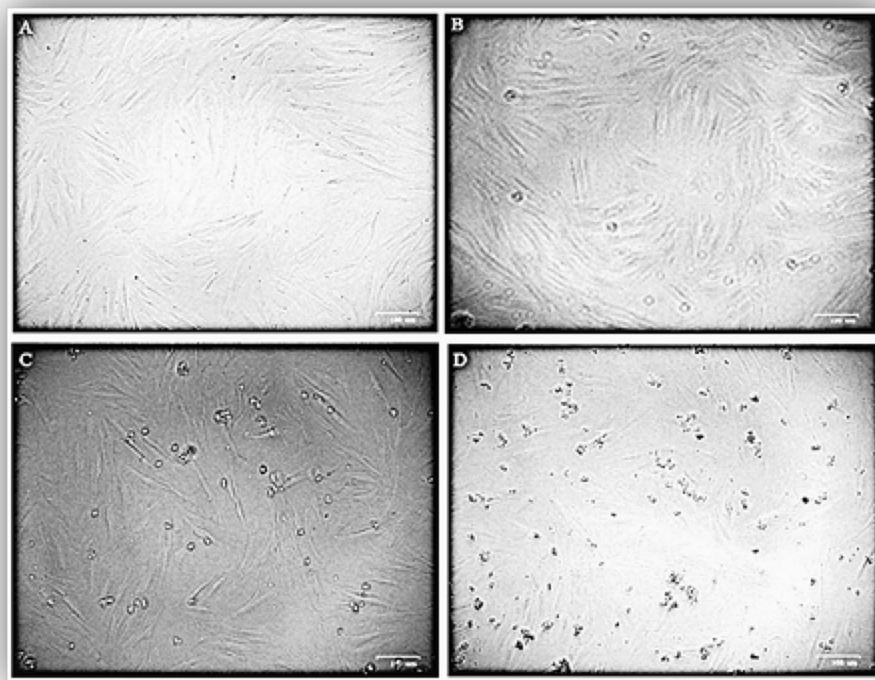


Figure 3. Morphology of fibroblast cells; (a) Control cells, (b) Cells treated with 3.12 µg/ml, (c) 6.25 µg/ml, (d) 12.5 µg/ml of the isolated compound.

| Concentration (µg/ml) | HRBC membrane stabilization | |
|--------------------------|-----------------------------|--------------|
| | Isolated compound | Diclofenac |
| 10 | 99.01 | 95.18 |
| 25 | 98.95 | 95.06 |
| 50 | 97.81 | 94.84 |
| 75 | 96.59 | 94.08 |
| 100 | 96.31 | 93.21 |
| IC ₅₀ (µg/ml) | 51.92 ± 0.03 ^b | 53.64 ± 0.01 |

Table 2. The anti-inflammatory activity of the isolated compound. Reported values are the mean ± SD (n = 3). Means in the same row followed by different lower case letters are significantly different (p < 0.05).

| | COVID-19 main protease | NSP10 | RNA-dependent RNA polymerase |
|-------------------------------------|------------------------|---------|------------------------------|
| The isolated compound | - 24.68 | - 23.47 | - 29.86 |
| Co-crystallized ligand (PRD_002214) | - 27.72 | - | - |
| Co-crystallized ligand (SAM) | - | - 17.86 | - |
| Co-crystallized ligand (F86) | - | - | - 23.56 |

Table 3. The docking binding free energies of the isolated compound and the co-crystallized ligands against SARS-CoV-2 target proteins.

formed many hydrophobic, electrostatic, and hydrogen bonding interactions with Asp6897, Lys6968, Lys6844, and Asp6928 (supplementary Fig. S11).

With respect to the binding mode of the co-crystallized ligand (F86) against COVID-19 RNA-dependent RNA polymerase, it formed three hydrogen bonds, six hydrophobic interactions, and two electrostatic interactions. Furthermore, the pyrrolo[2,1-f] [1,2,4] triazin-4-amine moiety formed six hydrophobic interactions with Urd20,

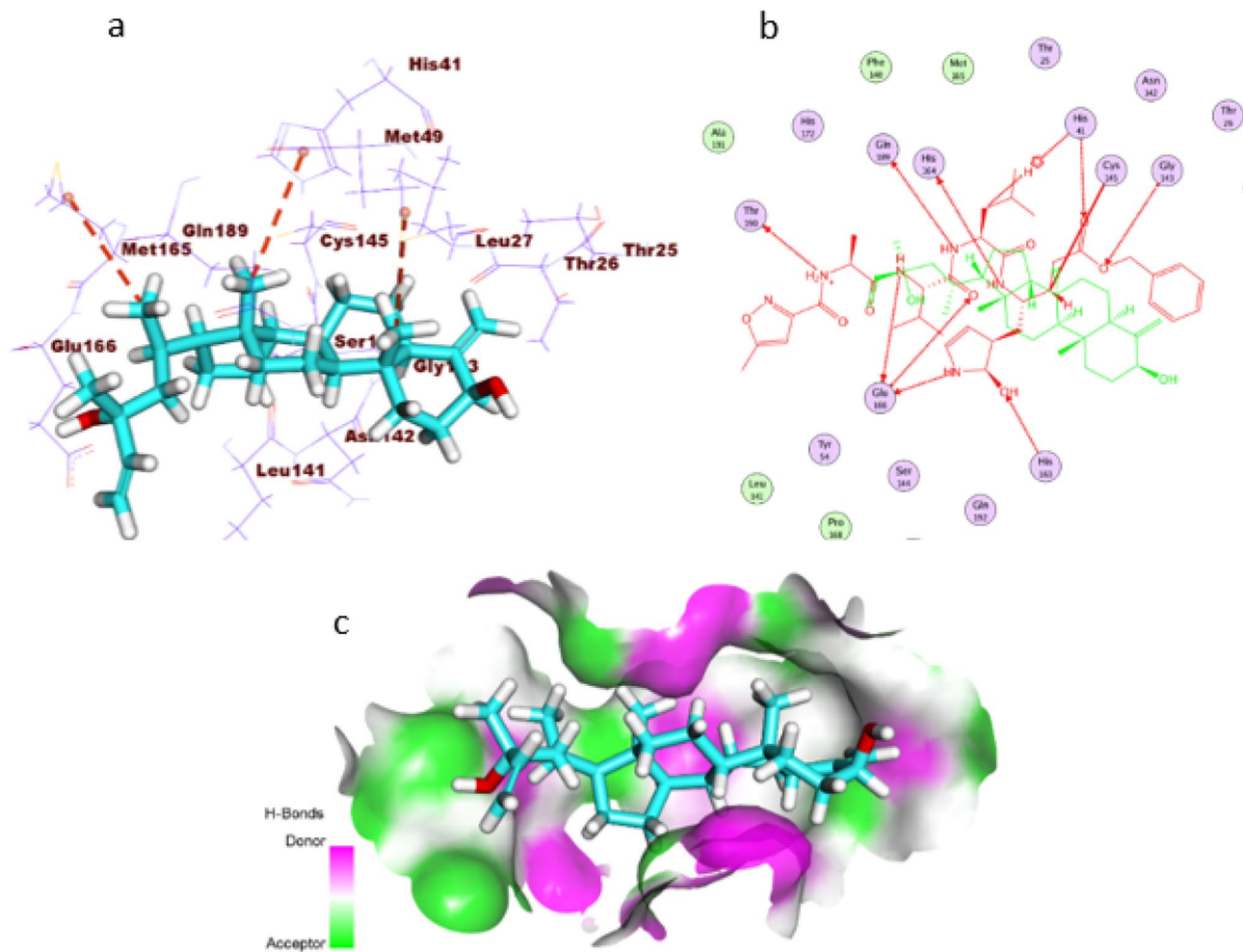


Figure 4. (a) 3D of the isolated compound docked into the active site of COVID-19 main protease. (b) 2D of the compound docked into the active site of COVID-19 main protease and superimposed with the co-crystallized ligand. (c) Mapping surface showing the compound occupying the active pocket of COVID-19 main protease.

Ade11, Arg555, and Val557. As well, the sugar moiety formed a hydrogen bond with Asp623. Additionally, the phosphate derivative moiety formed two electrostatic interactions and a hydrogen bond with Asp760, Asp623, and Cys622 (supplementary Fig. S12).

Considering the isolated compound's binding mode against the COVID-19 main protease protein, it occupied three pockets of the protein with a similar orientation to that of the co-crystallized ligand inside the active pocket of M^{pro} . Exhaustively, the (S)-2-methylenecyclohexan-1-ol moiety occupied the first pocket of M^{pro} , forming one hydrophobic interaction with Met49. Moreover, the (3aR,7aS)-3a-methyloctahydro-1H-indene moiety was buried in the second pocket, forming a hydrogen bond with His41. In addition, the (R)-3-methylhex-1-en-3-ol moiety was incorporated in hydrophobic interaction with Met165 in the third pocket of M^{pro} (Fig. 4).

The compound's interaction with the active pocket of NSP10 formed three hydrophobic interactions and a hydrogen bond. Closely, the hydroxyl group of (S)-2-methylenecyclohexan-1-ol moiety formed a hydrogen bond Asp6912. Such moiety formed two hydrophobic interactions with Leu6898. In addition, the (3aR,7aS)-3a-methyloctahydro-1H-indene moiety formed one hydrophobic interaction with Pro6932. The orientation of the compound inside the active pocket is similar to that of the co-crystallized ligand to some extent (Fig. 5).

The binding mode of the compound against RNA-dependent RNA polymerase formed twelve hydrophobic interactions and two hydrogen bonds with the active pocket. Comprehensively, the hydroxyl group of (S)-2-methylenecyclohexan-1-ol moiety formed two hydrogen bonds with Thr680 and Cys622. Such moiety formed a hydrophobic interaction with Urd20. Additionally, the (3aR,7aS)-3a-methyloctahydro-1H-indene moiety formed five hydrophobic interactions with Urd20 and Ade11, whereas the (R)-3-methylhex-1-en-3-ol moiety formed five hydrophobic interactions with Lys545, Urd10, Val557, and Ala547 (Fig. 6).

ADMET studies were carried out for the isolated compound using lopinavir as a reference compound. Discovery studio 4.0 was used to predict the following ADMET descriptors; blood–brain barrier (BBB) penetration, aqueous solubility, intestinal absorption, hepatotoxicity, cytochrome P450 inhibition, and plasma protein binding. The predicted descriptors are listed in (Table 4).

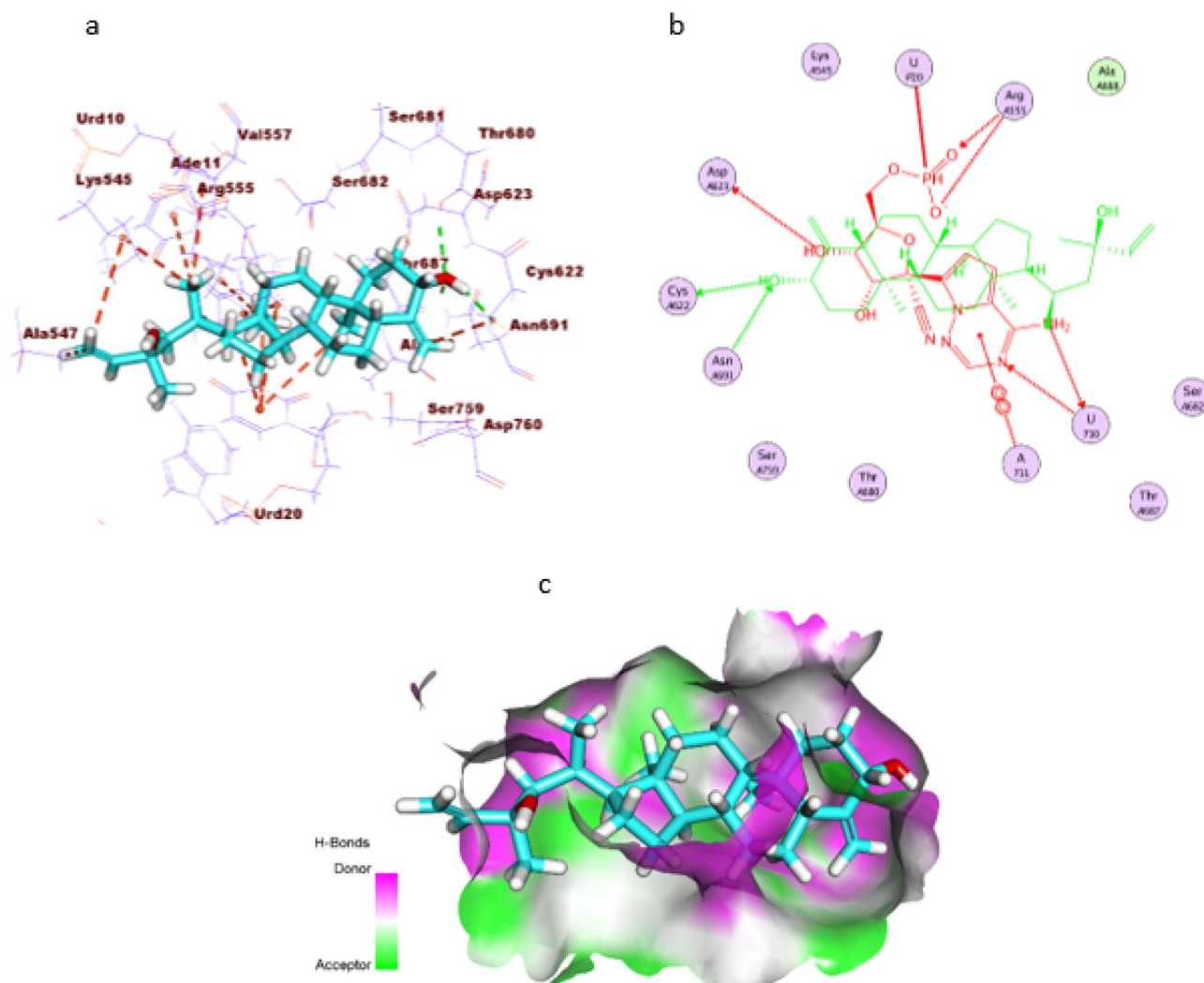


Figure 6. (a) 3D of the isolated compound docked into the active site of COVID-19 RNA-dependent RNA polymerase. (b) 2D of the compound docked into the active site of COVID-19 RNA-dependent RNA polymerase and superimposed with the co-crystallized ligand. (c) Mapping surface demonstrating the compound occupying the active pocket of COVID-19 RNA-dependent RNA polymerase.

| | BBB level ^a | Solubility level ^b | Absorption level ^c | CYP2D6 prediction ^d | Hepatotoxicity | PPB prediction ^e |
|-----------------------|------------------------|-------------------------------|-------------------------------|--------------------------------|----------------|-----------------------------|
| The isolated compound | 0 | 1 | 0 | False | False | True |
| Lopinavir | 4 | 3 | 2 | False | True | True |

Table 4. The predicted ADMET for the isolated compound and lopinavir. ^a0 = very high, 1 = high, 2 = medium, 3 = low, 4 = very low. ^b1 = very low, 2 = low, 3 = good, 4 = optimal. ^c0 = good, 1 = moderate, 2 = poor, 3 = very poor. ^dTRUE = inhibitor, FALSE = non inhibitor. ^eFALSE means less than 90%, TRUE means more than 90%.

inhibitory effect at concentration 10.4 μM , suggesting that our isolated compound is a promising viral inhibitor against SARS-CoV2 and its mode of action could be during the viral replication or had a virucidal effect.

The results revealed that the isolated compound has low toxicity to normal cells and could be used as an antiviral agent after performing in vivo assays. Interestingly, the effective dose which inhibited 95% of the viral count was 5 ng/ μl (5 $\mu\text{g}/\text{ml}$) and that below the IC_{50} value (11.35 \pm 1.5 $\mu\text{g}/\text{ml}$) of the normal fibroblast cells. The obtained IC_{50} for the isolated compound was lowered than the reference drug (Diclofenac), indicating that the compound was more potent than diclofenac and could be used as an anti-inflammatory drug.

Echinoderms are rich bioactive components that provide tremendous pharmaceutical and clinical medicine values. Similarly, like many marine invertebrates, survival requirements have led to the evolution of these complex substances. Interestingly, several secondary metabolites were proven to have a potent antiviral activity as well as a relatively non-cytotoxicity. As a result, these promising echinoderm natural compounds could be used to

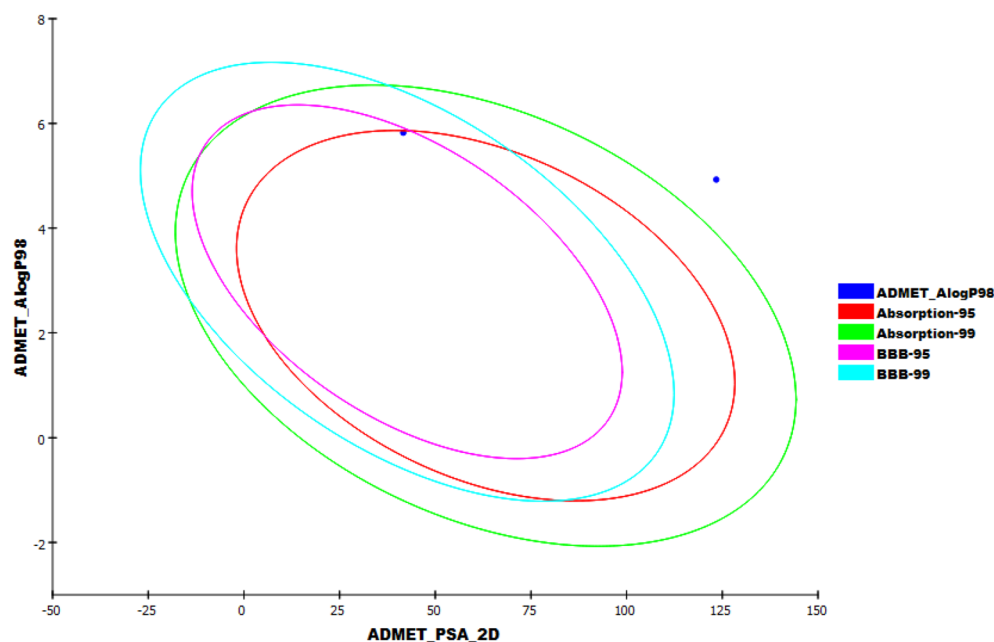


Figure 7. The expected ADMET study.

| | FDA rodent carcinogenicity (rat-male) | Carcinogenic potency TD ₅₀ (rat) ^a | Rat maximum tolerated dose (feed) ^b | Rat oral LD ₅₀ ^b | Rat chronic LOAEL ^b | Ocular irritancy | Skin irritancy |
|-----------------------|---------------------------------------|--|--|--|--------------------------------|------------------|----------------|
| The isolated compound | Non-carcinogen | 0.621 | 0.040 | 1.715 | 0.002 | Irritant | Moderate |
| Lopinavir | Non-carcinogen | 3.553 | 0.117 | 1.154 | 0.049 | Irritant | None |

Table 5. The isolated compound's toxicity properties. ^aUnit: mg/kg body weight/day. ^bUnit: g/kg body weight.

develop new antiviral drugs. In this study, 5 α -cholesta-4(27), 24-dien-3 β , 23 β -diol was isolated from the brittle stars, *Ophiocoma dentata* showing 95% inhibition of COVID-19 virus at concentration 5 ng/ μ l, which is safe to the normal cells. The current study's findings are promising regarding finding an effective cure for the COVID-19 pandemic. Further in-vivo studies regarding the clinical and structure-activity relationship are needed to confirm the isolated compound's potential against the infectious virus SARS-CoV-2.

Marine natural products remain a promising source for discovering high structural diversity and various bioactivities that can be directly developed or used as starting points for the development of novel medications. In the future, we must consider the final dosage form for human use (e.g., tablets, capsules, and injections) to have the potential to be translated into a clinically applicable therapeutic. Biological challenges, large-scale manufacturing, biocompatibility, intellectual property, stable storage, government regulations, and overall cost-effectiveness should all be considered during clinical development. Future research could focus on determining the biodistribution, Pharmacodynamics, and pharmacokinetics in humans, as well as screening for safety and demonstrating the preliminary efficacy of the isolated compound. It is critical to comprehend how the in-vivo environment influences its long-term structural organization, retention, and clearance.

Methods

Sample collection. Live Brittle star; *O. dentata* with body weight (50–200 g) were collected in June 2019 from the Red Sea shore at Hurghada, Egypt, from the tidal zone in front of the Marine biological station (NIOF), at about 4–10 m deep between latitude 27.28°N and longitude 33.77° E. This species is among the most abundant brittle star observed in the area. Samples were identified according to their morphological characteristics with taxonomic reference²⁸. Voucher specimens (2019-618MS) have been deposited at the National Institute of Oceanography and Fisheries, Egypt. Samples were washed, packed in polypropylene bags, and immediately frozen before being transported to the laboratory and stored at – 20 °C until use.

Extraction and isolation. The whole bodies of brittle star *O. dentata* (1 kg) were extracted with CHCl₃/MeOH at room temperature three times then concentrated under reduced pressure until they were dried. The resultant residue was kept frozen at – 20 °C for further purification and analysis. The crude extract (14.62 g) of brittle star (*O. dentata*) was subjected to (1st) column packed with silica gel size of 60–200 μ m (70–230 mesh) and elution via mobile phase Hexane: DCM (100:0%) then (95:5%) and increasing the polarity until reaching

(0:100%). Consequently, 250 fractions were collected, and fractions with the same RF value were combined to give 32 fractions, as shown in supplementary Fig. S1.

Finally, we isolated a new compound namely 5 α -cholesta-4(27), 24-dien-3 β , 23 β -diol (Fig. 1) from *O. dentata* with TLC (DCM: MeOH, 99:1 v/v): R_f=0.53; ¹H NMR (400 MHz, CDCl₃): δ 1.05 (m, 2H), 1.80 (m, 2H), 1.06 (d, J = 10 Hz, 3H), 2.04 (d, J = 8.8 Hz, 2H), 5.93 (m, 1H), 5.09 (d, J = 10.8 Hz, 2H), 5.23 (d, J = 17.2 Hz, 2H), 1.44 (s, 3H), 4.67 (s, 2H), 4.93 (s, 2H); ¹³C NMR (125 MHz, CDCl₃): δ 145.6, 145.1, 111.7, 109.1, 73.3, 67.3, 53.2, 46.1, 41.3, 37.1; IR: 3424 cm⁻¹, 1742 cm⁻¹; HREIMS (m/z): C₂₇H₄₄O₂, 400.6470.

Spectroscopic characterization of the isolated compound. *NMR analysis.* The ¹H NMR and ¹³C NMR analysis was measured at Bruker AVANCE 400 MHz NMR spectrometers at the University of Winnipeg, Canada, using Deuterated chloroform (CDCl₃). COSY, HSQC, HMBC, and NOESY were also measured. Chemical shift (δ) values were given in ppm while coupling constants (J) in Hz.

FT-IR analysis. The compound's functional groups were identified using infrared spectroscopy. The powdered compound was mixed 1:1 with dried KBr powder to make a compressed pellet using the Bruker Alpha Fourier transform infrared spectroscopy spectrometer with the subsequent recording of infrared spectrum in the transmission mode from 4000 to 400 cm⁻¹.

GC-MS analysis. The compound was subjected to GC-MS to identify and confirm the structure of the purified bioactive compound. The sample was analyzed in an Agilent 7890A-5975C high-resolution gas chromatography-mass spectroscopy instrument. The carrier gas was Helium, and the analysis was performed at 90–300 °C. The identification and confirmation of the structure of the compound were made using computer matching of spectral data with that of standards.

Molecular docking analysis of isolated compound. The target proteins' crystal structures: (i) Main protease of COVID-19 (M^{pro}) (PDB ID: 6lu7, resolution: 2.16 Å), (ii) non-structural protein (nsp10) (PDB ID: 6W4H, resolution: 1.80 Å), and (iii) RNA-dependent RNA polymerase (PDB ID: 7BV2, resolution: 2.50 Å) were downloaded from Protein Data Bank (<http://www.pdb.org>). Molecular Operating Environment (MOE) was used for the docking analysis²⁹. The free energies and binding modes of the tested molecules against target proteins were established in this investigation. Water molecules were first eliminated from target proteins crystal structures, leaving only one chain required for binding. The reference ligands were co-crystallized. The hydrogen atoms were then hidden, and the protein structures were protonated. Afterward, the MMFF94x force field was used to reduce the energy. After that, the binding pockets of each protein were defined^{30–32}.

ChemBioDraw Ultra 14.0 was used to draw the structure of the investigated compound and the co-crystallized ligands, which were saved as SDF formats. Subsequently, the stored files were opened using MOE software, and 3D structures were protonated. The MMFF94x force field was then applied to minimize the energy of the molecules. Validation processes for each target receptor were carried out by running the docking process for only the co-crystallized ligand. Valid performance is indicated by low RMSD values between docked and crystal conformations^{33,34}. The output from the MOE software was further analyzed and visualized using the Discovery Studio 4.0 software^{35–38}.

In silico ADMET analysis. Discovery studio 4.0 was used to determine the compound's ADMET descriptors (absorption, distribution, metabolism, excretion, and toxicity). According to the small molecule preparation protocol, the compound was prepared and minimized after applying the CHARMM force field. These studies were then carried out using the ADMET descriptors procedure^{33,36}.

In silico toxicity studies. Discovery studio 4.0 was used to calculate the toxicity parameters of the isolated compound. Lopinavir was used as a reference drug. The toxicity prediction (extensible) protocol calculated various parameters^{36,39,40}.

Determination of anti-SARS-CoV2 activity. In order to evaluate the antiviral activity of the isolated compound, the plaque reduction assay was carried out according to Mustafa et al.²⁷ at the main laboratories of chemical warfare in Egypt. Percentage reduction in plaques formation in comparison to control wells was recorded as follows:

$$\% \text{ inhibition} = \frac{\text{viral count (untreated)} - \text{viral count (treated)}}{\text{viral count (untreated)}} \times 100$$

MTT cytotoxicity assay. MTT assay, an in-vitro cytotoxicity test, was used to measure cell viability and membrane damage following van de Loosdrecht et al.⁴¹. Sample dissolved in 10% DMSO, then tested against human gingival fibroblast cell lines (obtained as a gift from faculty of medicine, Egypt) by using 3-(4,5-dimethylthiazol-2-yl)-2,5-diphenyltetrazolium bromide (MTT). A microplate reader (ASYS-EXPERT 96) was utilized to measure the optical density at 540 nm. The changes in the morphology of cells exposed to the isolated compound were monitored using inverted microscopy and Biorad (ZOE fluorescent cell imager).

Anti-inflammatory activity. The isolated compound's anti-inflammatory activity in-vitro was assessed by the human red blood corpuscles (HRBCs) membrane-stabilizing method⁴². The percentage membrane stabilization was calculated using the following formula:

$$\% \text{ Protection} = 100 - \frac{\text{OD of test}}{\text{OD of control}} \times 100$$

Statistical analysis. SPSS version 16 was used to analyze the data obtained using one-way analysis of variance (ANOVA). Values are expressed as mean \pm SD (n = 3). P values \leq 0.05 were considered significant.

Data availability

All data generated or analyzed during this study are included in this published article (and its Supplementary Information files).

Received: 17 November 2021; Accepted: 25 March 2022

Published online: 07 April 2022

References

- Rivero-Segura, N. A. & Gomez-Verjan, J. C. In silico screening of natural products isolated from Mexican herbal medicines against COVID-19. *Biomolecules* **11**, 216 (2021).
- Harrison, C. Coronavirus puts drug repurposing on the fast track. *Nat. Biotechnol.* **38**, 379–381 (2020).
- Khalifa, S. A. M. *et al.* Screening for natural and derived bio-active compounds in preclinical and clinical studies: One of the frontlines of fighting the coronaviruses pandemic. *Phytomedicine* **85**, 153311 (2021).
- El-Seedi, H. R. *et al.* Plants mentioned in the Islamic Scriptures (Holy Qur'an and Ahadith): Traditional uses and medicinal importance in contemporary times. *J. Ethnopharmacol.* **243**, 112007 (2019).
- Blunt, J. W., Copp, B. R., Keyzers, R. A., Munro, M. H. G. & Prinsep, M. R. Marine natural products. *Nat. Prod. Rep.* **31**, 160–258 (2014).
- Sudek, S. *et al.* Identification of the putative bryostatin polyketide synthase gene cluster from 'Candidatus Endobugula sertula', the uncultivated microbial symbiont of the marine bryozoan Bugula neritina. *J. Nat. Prod.* **70**, 67–74 (2007).
- Fayed, M. A. A. *et al.* Structure- and ligand-based in silico studies towards the repurposing of marine bioactive compounds to target SARS-CoV-2. *Arab. J. Chem.* **14**, 103092 (2021).
- Lee, J. *et al.* A new 2,3-dimethyl butenolide from the brittle star Ophiomastix mixta. *Chem. Pharm. Bull.* **55**, 459–461 (2007).
- Murgueitio, M. S., Bermudez, M., Mortier, J. & Wolber, G. In silico virtual screening approaches for anti-viral drug discovery. *Drug Discov. Today Technol.* **9**, e219–e225 (2012).
- Raj, U. & Varadwaj, P. K. Flavonoids as multi-target inhibitors for proteins associated with ebola virus: In silico discovery using virtual screening and molecular docking studies. *Interdiscip. Sci. Comput. Life Sci.* **8**, 132–141 (2016).
- Gao, Y. *et al.* Structure of the RNA-dependent RNA polymerase from COVID-19 virus. *Science* **368**, 779–782 (2020).
- Jin, Z. *et al.* Structure of Mpro from SARS-CoV-2 and discovery of its inhibitors. *Nature* **582**, 289–293 (2020).
- Dai, W. *et al.* Structure-based design of antiviral drug candidates targeting the SARS-CoV-2 main protease. *Science* **368**, 1331–1335 (2020).
- Sayed, A. M. *et al.* Nature as a treasure trove of potential anti-SARS-CoV drug leads: A structural/mechanistic rationale. *RSC Adv.* **10**, 19790–19802 (2020).
- Shaldam, M. A., Yahya, G., Mohamed, N. H., Abdel-Daim, M. M. & Al Naggar, Y. In silico screening of potent bioactive compounds from honeybee products against COVID-19 target enzymes. *Environ. Sci. Pollut. Res.* <https://doi.org/10.1007/s11356-021-14195-9> (2021).
- Yang, X. W. *et al.* Isolation and structural characterisation of five new and 14 known metabolites from the commercial starfish *Archaster typicus*. *Food Chem.* **124**, 1634–1638 (2011).
- Popov, R. S. *et al.* Aphelasteroside F, a new asterosaponin from the far eastern starfish *Aphelasterias japonica*. *Nat. Prod. Commun.* **11**, 1934578X1601100913 (2016).
- Xia, X., Maliski, E. G., Gallant, P. & Rogers, D. Classification of kinase inhibitors using a Bayesian model. *J. Med. Chem.* **47**, 4463–4470 (2004).
- BIOVIA. QSAR, ADMET and Predictive Toxicology. <https://www.3dsbiovia.com/products/collaborative-science/biovia-discovery-studio/qsar-admet-and-predictive-toxicology.html> (2020).
- Venkatapathy, R., Wang, N. C. Y., Martin, T. M., Harten, P. F. & Young, D. Structure-activity relationships for carcinogenic potential. *Gen. Appl. Toxicol.* <https://doi.org/10.1002/9780470744307.gat079> (2009).
- Goodrnan, G. & Wilson, R. Comparison of the dependence of the TD50 on maximum tolerated dose for mutagens and nonmutagens. *Risk Anal.* **12**, 525–533 (1992).
- Krewski, D., Gaylor, D. W., Soms, A. P. & Szyszkwicz, M. An overview of the report: Correlation between carcinogenic potency and the maximum tolerated dose: Implications for risk assessment. *Risk Anal.* **13**, 383–398 (1993).
- Diaza, R. G. *et al.* Comparison of in silico tools for evaluating rat oral acute toxicity. *SAR QSAR Environ. Res.* **26**, 1–27 (2015).
- Pizzo, F. & Benfenati, E. In silico models for repeated-Dose Toxicity (RDT): Prediction of the No Observed Adverse Effect Level (NOAEL) and Lowest Observed Adverse Effect Level (LOAEL) for drugs. In *Methods in Molecular Biology* Vol. 1425 (2016).
- Venkatapathy, R., Moudgal, C. J. & Bruce, R. M. Assessment of the oral rat chronic lowest observed adverse effect level model in TOPKAT, a QSAR software package for toxicity prediction. *J. Chem. Inf. Comput. Sci.* **44**, 1623–1629 (2004).
- Wilhelmus, K. R. The Draize eye test. *Surv. Ophthalmol.* **45**, 493–515 (2001).
- Mostafa, A. *et al.* Fda-approved drugs with potent in vitro antiviral activity against severe acute respiratory syndrome coronavirus 2. *Pharmaceuticals* **13**, 443 (2020).
- Gondim, A., Alonso, C., Pereira Dias, T. L., de Castro Manso, C. L. & Lindsey Christoffersen, M. A taxonomic guide to the brittle-stars (Echinodermata, Ophiuroidea) from the State of Paraíba continental shelf, Northeastern Brazil. *Zookeys* **307**, 45 (2013).
- Martins, N., Petropoulos, S. & Ferreira, I. C. F. R. Chemical composition and bioactive compounds of garlic (*Allium sativum* L.) as affected by pre- and post-harvest conditions: A review. *Food Chem.* **211**, 41–50 (2016).
- El-Gamal, K. M., El-Morsy, A. M., Saad, A. M., Eissa, I. H. & Alswah, M. Synthesis, docking, QSAR, ADMET and antimicrobial evaluation of new quinoline-3-carbonitrile derivatives as potential DNA-gyrase inhibitors. *J. Mol. Struct.* **1166**, 15–33 (2018).
- Li, N. *et al.* Screening of some sulfonamide and sulfonyleurea derivatives as anti-Alzheimer's agents targeting BACE1 and PPAR γ . *J. Chem.* **2020** 1–19 (2020).

32. Hagra, M. *et al.* Discovery of new quinolines as potent colchicine binding site inhibitors: Design, synthesis, docking studies, and anti-proliferative evaluation. *J. Enzyme Inhib. Med. Chem.* **36**, 640–658 (2021).
33. Ibrahim, M. K. *et al.* Design, synthesis, molecular modeling and anti-hyperglycemic evaluation of quinazolin-4(3H)-one derivatives as potential PPAR γ and SUR agonists. *Bioorganic Med. Chem.* **25**, 4723–4744 (2017).
34. Elmetwally, S. A., Saied, K. F., Eissa, I. H. & Elkaeed, E. B. Design, synthesis and anticancer evaluation of thieno[2,3-d]pyrimidine derivatives as dual EGFR/HER2 inhibitors and apoptosis inducers. *Bioorg. Chem.* **88**, 102944 (2019).
35. Mahdy, H. A. *et al.* Design, synthesis, molecular modeling, in vivo studies and anticancer evaluation of quinazolin-4(3H)-one derivatives as potential VEGFR-2 inhibitors and apoptosis inducers. *Bioorg. Chem.* **94**, 103422 (2020).
36. El-Zahabi, M. A. *et al.* Design, synthesis, molecular modeling and anti-hyperglycemic evaluation of phthalimide-sulfonylurea hybrids as PPAR γ and SUR agonists. *Bioorg. Chem.* **91**, 103115 (2019).
37. El-Naggar, A. M., Eissa, I. H., Belal, A. & El-Sayed, A. A. Design, eco-friendly synthesis, molecular modeling and anticancer evaluation of thiazol-5(4H)-ones as potential tubulin polymerization inhibitors targeting the colchicine binding site. *RSC Adv.* **10**, 2791–2811 (2020).
38. Nasser, A. A. *et al.* Discovery of new pyrimidine-5-carbonitrile derivatives as anticancer agents targeting EGFRWTand EGFR790M. *Org. Biomol. Chem.* **18**, 7608–7634 (2020).
39. Alanazi, M. M. *et al.* New bis([1,2,4]triazolo)[4,3-a:3',4'-c]quinoxaline derivatives as VEGFR-2 inhibitors and apoptosis inducers: Design, synthesis, in silico studies, and anticancer evaluation. *Bioorg. Chem.* **112**, 104949 (2021).
40. Alesawy, M. S. *et al.* In silico studies of some isoflavonoids as potential candidates against COVID-19 targeting human ACE2 (hACE2) and viral main protease (Mpro). *Molecules* **26**, 2806 (2021).
41. van de Loosdrecht, A. A., Beelen, R. H. J., Ossenkuppe, G. J., Broekhoven, M. G. & Langenhuijsen, M. M. A. C. A tetrazolium-based colorimetric MTT assay to quantitate human monocyte mediated cytotoxicity against leukemic cells from cell lines and patients with acute myeloid leukemia. *J. Immunol. Methods* **174**, 311–320 (1994).
42. Anandarajagopal, K. In-vitro anti-inflammatory evaluation of crude *Bombax ceiba* extracts. *Eur. J. Med. Plants* **3**, 99 (2013).

Acknowledgements

We thank the Department of Chemistry, University of Winnipeg, Canada, where the elucidation of structures was completely achieved under the supervision of Prof. Athar Ata.

Author contributions

M.S.M.A.E.H., M.A.E.D., and D.A.G. conceptualized and designed the study. M.S.M.A.E.H. performed the isolation and structure elucidation. M.G.A. performed the anti-inflammation activity assay. A.S.A.A. performed the MTT assay. M.G.S., M.F.E., and O.B. performed the anti-COVID-19 assay. M.S.M.A.E.H. wrote the original draft. M.S.M.A.E.H., M.A.E.D., and D.A.G. contributed to writing and editing the manuscript. The final manuscript was read and approved by all authors.

Funding

Open access funding provided by The Science, Technology & Innovation Funding Authority (STDF) in cooperation with The Egyptian Knowledge Bank (EKB).

Competing interests

The authors declare no competing interests.

Additional information

Supplementary Information The online version contains supplementary material available at <https://doi.org/10.1038/s41598-022-09809-2>.

Correspondence and requests for materials should be addressed to M.S.M.A.E.

Reprints and permissions information is available at www.nature.com/reprints.

Publisher's note Springer Nature remains neutral with regard to jurisdictional claims in published maps and institutional affiliations.



Open Access This article is licensed under a Creative Commons Attribution 4.0 International License, which permits use, sharing, adaptation, distribution and reproduction in any medium or format, as long as you give appropriate credit to the original author(s) and the source, provide a link to the Creative Commons licence, and indicate if changes were made. The images or other third party material in this article are included in the article's Creative Commons licence, unless indicated otherwise in a credit line to the material. If material is not included in the article's Creative Commons licence and your intended use is not permitted by statutory regulation or exceeds the permitted use, you will need to obtain permission directly from the copyright holder. To view a copy of this licence, visit <http://creativecommons.org/licenses/by/4.0/>.

© The Author(s) 2022